



**HAL**  
open science

## The Kinesin Light Chain–Related Protein PAT1 Promotes Superoxide Anion Production in Human Phagocytes

Riad Arabi-Derkawi, Yvonne O’dowd, Ni Cheng, Loïc Rolas, Tarek Boussetta, Houssam Raad, Viviana Marzaioli, Coralie Pintard, Magali Fasseu, Yolande Kroviarski, et al.

► **To cite this version:**

Riad Arabi-Derkawi, Yvonne O’dowd, Ni Cheng, Loïc Rolas, Tarek Boussetta, et al.. The Kinesin Light Chain–Related Protein PAT1 Promotes Superoxide Anion Production in Human Phagocytes. *Journal of Immunology*, 2019, 202 (5), pp.1549-1558. 10.4049/jimmunol.1800610 . hal-03014701

**HAL Id: hal-03014701**

**<https://hal.science/hal-03014701>**

Submitted on 19 Nov 2020

**HAL** is a multi-disciplinary open access archive for the deposit and dissemination of scientific research documents, whether they are published or not. The documents may come from teaching and research institutions in France or abroad, or from public or private research centers.

L’archive ouverte pluridisciplinaire **HAL**, est destinée au dépôt et à la diffusion de documents scientifiques de niveau recherche, publiés ou non, émanant des établissements d’enseignement et de recherche français ou étrangers, des laboratoires publics ou privés.

1 **The kinesin light-chain-related protein PAT1 promotes superoxide anion production in**  
2 **human phagocytes**

3

4 **Running title:** PAT1 is a new regulator of the phagocyte NADPH oxidase

5

6 **Riad Arabi-Derkawi**<sup>†,‡,§\*</sup>, **Yvonne O'Dowd**<sup>†,‡,||\*</sup>, **Ni Cheng**<sup>¶</sup>, **Loïc Rolas**<sup>†,‡</sup>, **Tarek**  
7 **Boussetta**<sup>†,‡</sup>, **Houssam Raad**<sup>†,‡</sup>, **Viviana Marzaioli**<sup>†,‡</sup>, **Coralie Pintard**<sup>†,‡</sup>, **Magali Fasseu**<sup>†,‡</sup>,  
8 **Yolande Kroviarski**<sup>†,‡</sup>, **Sahra A. Belambri**<sup>†,‡,#</sup>, **Pham My-Chan Dang**<sup>†,‡</sup>, **Richard D. Ye**<sup>¶</sup>,  
9 **Marie-Anne Gougerot-Pocidal**<sup>†,‡,§</sup> and **Jamel El-Benna**<sup>†,‡</sup>.

10

11

12 <sup>†</sup> Inserm, U1149, CNRS-ERL8252, Centre de Recherche sur l'Inflammation, 75018 Paris,  
13 France

14

15 <sup>‡</sup> Université Paris Diderot, Sorbonne Paris Cité, Laboratoire d'Excellence Inflammex, Faculté de  
16 Médecine, Site Xavier Bichat, 75018 Paris, France

17

18 <sup>§</sup> AP-HP, Centre Hospitalier Universitaire Xavier Bichat, UF Dysfonctionnements  
19 Immunitaires, Paris, F-75018, France

20

21 <sup>¶</sup> University of Illinois College of Medicine, Chicago, IL 60612 USA.

22 <sup>||</sup> Forensic Science Ireland, Garda Headquarters, Phoenix Park, Dublin 8, Ireland

23 <sup>#</sup> Laboratoire de Biochimie appliquée, Faculté des Sciences de la Nature et de la Vie,  
24 Université Ferhat Abbas, Sétif, Algeria.

25

26

27  
28

29 **ABSTRACT**

30 Superoxide anion production by the phagocyte NADPH oxidase plays a crucial role in host  
31 defences and inflammatory reaction. The phagocyte NADPH oxidase is composed of  
32 cytosolic components (p40phox, p47phox, p67phox and Rac1/2) and the membrane  
33 flavocytochrome b558, which is composed of two proteins, p22phox and gp91phox/NOX2.  
34 P22phox plays a crucial role in the stabilization of gp91phox in phagocytes and is also a  
35 docking site for p47phox during activation. In the present study, we have used a yeast two-  
36 hybrid approach to identify unknown partners of p22phox. Using the cytosolic C-terminal  
37 region of p22phox as bait to screen a human spleen cDNA library, we identified the protein  
38 interacting with Amyloid Precursor Protein tail 1 (PAT1) as a potential partner of p22phox.  
39 The interaction between p22phox and PAT1 was further confirmed by *in vitro* GST pull-down  
40 and overlay assays and in intact neutrophils and COSphox cells by co-immunoprecipitation.  
41 We demonstrated that PAT1 is expressed in human neutrophils and monocytes and  
42 colocalizes with p22phox, as shown by confocal microscopy. Over-expression of PAT1 in  
43 human monocytes and in COSphox cells increased superoxide anion production and depletion  
44 of PAT1 by specific siRNA inhibited this process. These data clearly identify PAT1 as a  
45 novel regulator of NADPH oxidase activation and superoxide anion production, a key  
46 phagocyte function.

47

## 48 **Introduction**

49

50 Phagocytes such as polymorphonuclear neutrophils (PMN) and monocytes constitute a major  
51 defense line against pathogens, such as bacteria and fungi (1-3). At the site of infection,  
52 phagocytes recognize and phagocytose pathogens, a process that includes the formation of  
53 intracellular phagosomes and the destruction of the internalized pathogens (3,4). Activated  
54 PMNs and monocytes release antibacterial substances into the phagosome and produce  
55 superoxide anion from which derive other reactive oxygen species (ROS) that are thought to  
56 play an important role in both the direct and indirect killing of pathogens (4-6). The  
57 superoxide anion is the precursor of other ROS molecules, such as hydrogen peroxide and  
58 hypochlorous acid. In phagocytes, the enzyme responsible for superoxide production is the  
59 nicotinamide adenine dinucleotide phosphate reduced form (NADPH) oxidase or respiratory  
60 burst oxidase (7-11).

61 The phagocyte NADPH oxidase, is a multicomponent enzyme, comprising several subunits ;  
62 p22phox, p40phox, p47phox, p67phox, gp91phox (also called NOX2) and a small GTPase  
63 Rac1 or Rac2 (7-11). In the resting cell, p40phox, p47phox, p67phox exist in the cytosol as a  
64 complex, and Rac1 (in monocytes) or Rac2 (in neutrophils) exist in the GDP-bound form,  
65 complexed to Rho-GDI. The other two components p22phox and gp91phox form a non-  
66 covalently bound complex known as flavocytochrome b558 (7-11). They are located in the  
67 membranes of specific granules, gelatinase granules, secretory vesicles and the plasma  
68 membrane. Separating these two groups of components by distributing them between distinct  
69 subcellular compartments ensures that the NADPH oxidase is inactive in the resting cell.  
70 Upon cell activation by various stimuli, several events take place simultaneously, including  
71 phosphorylation and translocation of the cytosolic components p40phox, p47phox, p67phox  
72 to the membranes where they associate with the flavocytochrome b558 (12-18). Rac2

73 exchanges its GDP for GTP, dissociates from its inhibitor rho-GDI and migrates to the  
74 membrane where it interacts with p67phox. When all components are assembled at the  
75 membrane, the flavocytochrome b558, mediates the transfer of electrons from cytosolic  
76 NADPH to oxygen to produce the superoxide anion.

77 Human p22phox is a 195 amino acid protein; it has been proposed that the p22phox protein  
78 sequence consists of a short N-terminal tail, two transmembrane domains and a long C-  
79 terminal tail ranging from amino acids 130 to 195 (11). In resting cells, p22phox interacts  
80 with gp91phox, probably via the transmembrane spanning domains, to stabilize the complex.  
81 During activation, the intracellular cytosolic tail of p22phox interacts with p47phox *via* a  
82 “proline rich sequence/SH3 domains” docking site (19-21). Indeed, the p22phox C-terminal  
83 sequence has a polyproline sequence necessary for this interaction, as shown by site directed  
84 mutagenesis and in a CGD patient who has a mutation at proline 156 (22).

85 PAT1 is a 585 amino acid protein; it was first identified as a “protein interacting with  
86 Amyloid Precursor Protein (APP) tail”, via the basolateral sorting signal (BaSS) site in the  
87 cytoplasmic tail of APP, a cell surface protein implicated in the pathogenesis of Alzheimer  
88 disease (23). PAT1 is 99% and 99.6% identical to PAT1a and ARA67 respectively. PAT1 is  
89 expressed in several cells, such as epithelial cells and smooth muscle cells (24). PAT1 shares  
90 homology with kinesin light chain and was found to bind to microtubules, suggesting its  
91 implication in trafficking and protein secretion. Indeed, PAT1 and its isoform PAT1a were  
92 found to promote APP processing, resulting in increased secretion of beta-amyloid peptides  
93 (23,24). PAT1 was also found in the cytoplasm and the nucleus of MDCK (Madin-Darby  
94 canine kidney) cells and interacted and controlled the subcellular localisation of the androgen  
95 receptor, modulating its function (25,26). Whether PAT1 interacts with other proteins and  
96 regulates other cell functions is not known.

97 It is not known if gp91phox and p47phox are the only proteins interacting with p22phox  
98 under resting and activated conditions. We hypothesized that the cytosolic p22phox region  
99 could interact with new yet unidentified partners. In order to identify proteins that interact  
100 with p22phox, we performed a yeast two-hybrid screening of a human spleen cDNA library  
101 using the cytosolic C-terminal region of p22phox as bait. We have identified PAT1 as a novel  
102 p22phox interacting protein and shown it functions as an enhancer of NADPH oxidase  
103 activation and superoxide production in human phagocytes.

104

105

## 106 **Materials and Methods**

107

### 108 *Reagents*

109

110 Buffers, PMA, fMLF, C5a, phenylmethylsulfonylfluoride (PMSF), diisopropyl  
111 fluorophosphates (DFP), diphenyleneiodonium (DPI), the anti-actin monoclonal antibody and  
112 other chemicals were purchased from Sigma Aldrich (St. Louis, MO, USA). Sodium dodecyl  
113 sulfate-polyacrylamide gel electrophoresis (SDS-PAGE) and Western blotting reagents were  
114 purchased from Bio-Rad (Richmond, CA, USA). Dextran T500, Ficoll, G-sepharose beads,  
115 pGEX-6p1, and glutathione sepharose were purchased from GE Healthcare (Little Chalfont,  
116 UK). MACSxpress Neutrophil isolation Kit was from Miltenyi Biotec (Paris, France) and  
117 EasySep immunomagnetic negative selection kit was from Stemcell Technologies (Grenoble,  
118 france). A mouse polyclonal anti-PAT1 antibody raised against the last 100 amino acids (486  
119 a.a ~ 586 a.a) was from Abnova (Taipei, Taiwan). Anti-p22phox, anti-gp91phox antibodies  
120 were from Santa Cruz (Santa Cruz, CA, USA). Monoclonal anti-cytochrome b558 antibody

121 (7D5) was from MBL (Cliniscience, France). Secondary antibodies were from Jackson  
122 laboratories.

123

#### 124 *Two-hybrid Screening of human spleen cDNA library*

125

126 Two-hybrid screening was performed using the method described previously (27,28). The  
127 cDNA encoding the C-terminal tail of p22phox (residues 132-195) was cloned into the  
128 pLEX10 vector in frame with the LexA DNA-binding protein. The yeast strain L40  
129 established with the LexA-p22phox (residues 132-195) pLEX10 plasmid was transformed  
130 further with pACT2 plasmids containing cDNA's from a human spleen cDNA library  
131 (Clontech, Basingstoke, UK), fused with the sequence of the activation domain of Gal4. The  
132 transactivation of the two reporter genes His3 and LacZ was monitored firstly, by growth of  
133 transformed yeasts on selective medium lacking histidine, but also tryptophan and leucine.  
134 His<sup>+</sup> colonies were then assayed for  $\beta$ -galactosidase activity (LacZ<sup>+</sup>) by a qualitative colour  
135 filter assay (27,28). Recombinant pACT2 plasmids were recovered from His<sup>+</sup>/LacZ<sup>+</sup>  
136 phenotype yeasts, then amplified in E. Coli and finally sequenced.

137

#### 138 *Cloning and expression of human PAT1a and expression of the p22phox cytosolic domain* 139 *(residues 132-195) and the gp91cytosolic domain (residues 291-570)*

140

141 PAT1a cDNA contained in PKH3 plasmid (a generous gift from Dr. Stefan Kins, ZMBH,  
142 University of Heidelberg, Germany) was amplified using Pfu polymerase (Stratagene) with  
143 flanking ECOR1 and XhoI restriction sites open reading frame-flanking primers (sense, 5'-  
144 ccg gaa ttc atg gcg gcc gtg gaa cta -3'; antisense, 5'- ccg ctc gag tca gca gct cgg tcc ctc -3')  
145 and cloned into the pCRII-TOPO vector (Invitrogen). For recombinant expression of PAT1a,

146 the encoding cDNA was subcloned into pGEX-6P1 vector (Pharmacia, Piscataway, NJ, USA)  
147 and sequenced to rule out unexpected mutations and to confirm the sequence. It was then  
148 transformed in BL21-DE3 (pLysS) E. coli strain and expressed as follows. An overnight  
149 culture was diluted 10-fold in fresh Terrific Broth medium containing 100 µg/ml ampicillin  
150 and grown for one additional hour at 37°C. The culture was then induced with 0.2 mM  
151 isopropyl β-d-thiogalactoside for 18 h at 15°C. Bacteria were harvested by centrifugation  
152 (4000 g, 20 min, 4°C) and the pellet was resuspended in lysis buffer [50mM Tris-HCl (pH  
153 7.5), 50 mM NaCl, 5 mM MgCl<sub>2</sub>, 1 mM DTT, 1% (v/v) Triton X-100, protease-inhibitors].  
154 Cells were lysed by sonication (6 x 30 s), lysates were centrifuged (15000 g, 30 min, 4°C),  
155 GST-recombinant proteins were affinity precipitated from supernatant by overnight  
156 incubation at 4°C with glutathione-Sepharose 4B beads (Pharmacia). Beads were then washed  
157 in lysis buffer, and the fusion protein was cleaved by incubation with PreScission protease  
158 (Amersham Pharmacia) for 4-6 h at 4°C in 150 mM NaCl; 50 mM Tris-HCl, pH 7; 1 mM  
159 DTT; and 1 mM EDTA and subjected to another round of glutathione-bead adsorption.  
160 PAT1a (1-585) migrates at 67 kDa as a monomeric protein in a non denaturing gel.  
161 P22phox cDNA contained in a plasmid (a generous gift from Dr. Marry Dinauer, University  
162 of Saint Louis, USA). Cloning and expression of p22phox (aa132-195) cytoplasmic tail and  
163 gp91phox (aa 291-570) cytoplasmic tail in the pGEX-6P1 expression plasmid was performed  
164 as previously described (18,21).

165

166 *GST pull-down assay*

167

168 The assay was performed as described previously (18,29). Briefly, 80 pmol of GST-p22phox  
169 (132-195), GST-gp91phox (aa 291-570) and GST alone were incubated in the presence of 5  
170 pmol of recombinant PAT1 and glutathione-Sepharose beads in interaction buffer (20 mM

171 Hepes, pH 7.5; 1% Nonidet P-40; 50 mM NaCl; and 1 mM EGTA) for 1 h. After washing, the  
172 complex was eluted with 10 mM glutathione and analyzed by SDS-PAGE and Western blots  
173 using protein-specific antibodies.

174

#### 175 *Overlay assay*

176

177 Human recombinant PAT1 was subjected to SDS-PAGE and transferred to nitrocellulose  
178 membranes. Overlay with recombinant p22phox cytosolic tail was performed as we  
179 previously described (21).

180

#### 181 *Ethics statement*

182

183 Cells were isolated from the venous blood of healthy volunteers with their written informed  
184 consent in accordance with the Declaration of Helsinki. All experiments were approved by the  
185 INSERM Institutional Review Board and ethics committee. Data collection and analyses were  
186 performed anonymously.

187

#### 188 *Human neutrophil preparation and fractionation*

189

190 Human neutrophils were isolated from the blood of healthy volunteers by dextran  
191 sedimentation and ficoll centrifugation as described previously (30,31). The isolated cells  
192 were resuspended in phosphate-buffered saline at a concentration of  $10^8$  cells/ml in the  
193 presence or absence of DFP (2.7 mM) for 20 min at 15°C, and washed in the same buffer.  
194 Nuclei and cytoplasm were prepared using the NE-PER nuclear and cytoplasm extraction kit  
195 from Pierce (Rockford, IL, USA). For mRNA expression experiments, highly purified

196 neutrophils were obtained using the MACSxpress Neutrophil isolation Kit, and the EasySep  
197 immunomagnetic negative selection kit. These two kits yielded more than 99% purified  
198 neutrophils required for mRNA studies (32).

199

#### 200 *Human monocytes and lymphocytes isolation*

201

202 Peripheral blood mononuclear cells (PBMC) were freshly isolated from the whole blood of  
203 healthy volunteers by Ficoll-Paque separation (Pharmacia, Uppsala, Sweden) as previously  
204 described (30,31). PBMC were subjected to an additional separation step to isolate monocytes  
205 and lymphocytes (STEMCELL isolation kit). The purity of the resulting cell suspensions was  
206 randomly tested by a Sysmex XE-2100 automated blood cell counter (Sysmex, Kobe, Japan)  
207 and yielded more than 99% monocytes and 98% lymphocytes, respectively.

208

#### 209 *mRNA expression of PAT1 in human blood leukocytes*

210

211 Total RNAs were isolated by lysing the cells with Trizol reagent (Life Technologies)  
212 according to the manufacturer's instructions. Afterwards, 1µg of total RNAs were reverse  
213 transcribed and PAT1a mRNA was quantified by real-time polymerase chain reaction (RT-  
214 qPCR) using the Light Cycler Technology (Roche, Mannheim, Germany) and PAT1  
215 (covering a common part of the three isoforms) specific forward 5'- tgc aaa aag tca cta tga tga  
216 gg -3' and reverse 5'- tcc acc aca act ttc act gg -3' primers (Eurogentec). Detection of PCR  
217 product was based on SYBR green fluorescence signal. GAPDH house-keeping gene  
218 expression was used to normalise the results.

219

#### 220 *Cell lysate preparation for western blotting analysis*

221  
222 To detect PAT1 by western blotting in leukocytes, the cells were pretreated as following: cells  
223 were lysed in a lysis buffer (50 mM Tris-HCl buffer (pH 7.4), 1% Triton X-100, 2 mM  $\beta$ -  
224 glycerophosphate, 25 mM NaF, 150 mM NaCl, 10  $\mu$ g/ml each of Leupeptine, Pepstatine, and  
225 Aprotinine), then diluted twice with the same lysis buffer without Triton X-100, sonicated 3  
226 times for 3 seconds each and centrifugated for 5 min at 4000 rpm at 4°C. Protein  
227 concentration in the supernatant was determined prior to denaturation by addition of Laemmli  
228 sample buffer (2X) (31) and boiling at 100°C for 3 min.

229

### 230 *Transfection of PAT1 in COSphox cells*

231

232 COSphox cells which had been transfected with NADPH oxidase components (gp91phox,  
233 p22phox, p47phox and p67phox) were used to study the effect of PAT1 on NADPH oxidase  
234 activity in the resting state and following stimulation with fMLF, C5a or PMA (33,34). The  
235 cDNA for PAT1a fused to a hemagglutinin (HA) tag was subcloned into pRK5 vector.  
236 Lipofectamine 2000 reagent (Invitrogen) was used for transient transfection of expression  
237 vectors for human FPR1 (2.5  $\mu$ g), C5aR (2.5  $\mu$ g), P-Rex1 (0.5  $\mu$ g) and pRK5-PAT1a (1  $\mu$ g)  
238 into COSphox cells in a 100-mm culture dish ( $0.5-1 \times 10^6$  cells). Cells were analyzed 24 h  
239 later for superoxide anion production, based on isoluminol-enhanced chemiluminescence  
240 (CL) as previous described (33,34). The CL counts per second (cps) was continually recorded  
241 for 5–10 min before, and 20–30 min after stimulation with fMLF (1 $\mu$ M), C5a (100 nM) or  
242 PMA (200 ng/ml). The relative level of superoxide produced was calculated based on the  
243 integrated CL during the first 10 min after agonist stimulation. Whole cell lysate was prepared  
244 for Western blotting.

245

246 *Immunoprecipitation*

247

248 The technique used for cell lysis and cytochrome b558 immunoprecipitation was adapted  
249 from previously described protocols (15,18). Cells were lysed by resuspending ( $5 \times 10^7$   
250 cells/ml) in lysis buffer [50 mM Tris-HCl buffer (pH 7.4), 1% Triton X-100, 25 mM NaF, 2  
251 mM  $\beta$ -glycerophosphate, P8340 protease inhibitor cocktail (1:1,000 dilution), 150 mM NaCl,  
252 and 1 mM DFP]. Following sonication on ice and mixing by rotation, the lysates were  
253 centrifuged at 114,000 g for 30 min at 4°C. The supernatants were diluted twice in the same  
254 buffer without Triton X-100. Immunoprecipitation was performed by addition of anti-  
255 gp91phox or anti-p22phox or anti-cytochrome b558 or control IgG (1:200 dilution)  
256 monoclonal antibodies and protein A/G beads (Santa Cruz Biotech, Santa Cruz, CA, USA)  
257 saturated with BSA and incubated for 4 h. Beads were then washed 4 times, and proteins were  
258 denatured in sample buffer by boiling at 100°C for 3 min.

259

260 *Confocal microscopy*

261

262 Following treatment with fMLF or PMA, neutrophils were spotted using round gaped filter  
263 paper on poly-L-lysine-coated glass slides and allowed to dry in a humid chamber by gravity  
264 sedimentation, then fixed with 2% paraformaldehyde for 10 min, permeabilized with 0.2%  
265 Tween 20 for 15 min at 37°C and blocked with 5% BSA in PBS. Cells were then incubated  
266 overnight at 4°C with rabbit anti-p22phox polyclonal antibody (1:200) and mouse anti-PAT1  
267 monoclonal antibody (1:200) diluted in 1% BSA/PBS. After washing, cells were incubated  
268 with Alexa Fluor 488-(green)-conjugated goat anti-rabbit antibody (1:200) and Alexa Fluor

269 568 (red)-conjugated goat antimouse (1:200) for 1 h at room temperature in the dark. Nuclei  
270 were stained with TO-PRO-3 iodide (Invitrogen). Stained cells were examined with a Zeiss  
271 LSM510 confocal microscope (63/1.4 numerical aperture objective) and the images were  
272 imported into an LSM image browser for analysis. The designation 'Merge' corresponds to  
273 colocalisation of PAT1 and p22phox.

274

#### 275 *Pat1 silencing by siRNA in human monocytes*

276

277 To achieve PAT1 silencing, siRNAs (Santa Cruz, CA USA) was used. We used a liposome-  
278 based technology to deliver the nucleotides (35). Freshly isolated monocytes resuspended in  
279 RPMI without serum and antibiotics at the density of  $1.5 \times 10^6$  cells. Lipids (HiPerFect, Qiagen) and  
280 200 nM PAT1 siRNA were allowed to bind at the ratio of 1:1 (v/v) for 20 minutes at room  
281 temperature. The complex was then added to a new 6-well plate and then harvested cells were added  
282 dripping directly to the complex. Transfection was carried out for 4 hours, followed by addition of  
283 new complete RPMI media and cells were analysed 1-2 days later (35).

284

#### 285 *PAT1a overexpression in monocytes*

286

287 Transfection of human blood monocytes was performed in the Amaxa (Lonza, Cologne,  
288 Germany) system as recommended by the company. In brief, after centrifugation (1800 rpm  
289 for 8 min) monocytes were resuspended in supplemented human monocytes nucleofector®  
290 Solution (Amaxa) to a final concentration of  $5 \times 10^6$  cells/100  $\mu$ L; 100  $\mu$ L of cell suspension  
291 was mixed with 2  $\mu$ g of either pcDNA3.1-PAT1a plasmid or empty vector. After transfection

292 with the program Y-001, monocytes were seeded in 24-well plates at a density of  $5 \times 10^6$  cells  
293 per well in 2-ml supplemented medium and analysed after 24-36 hours of culture.  
294 Transfection efficiency was between 40% and 60% as verified by immunofluorescence.

295

296 *Measurement of superoxide anion production*

297

298 Monocytes ( $5 \times 10^5$ ) were suspended in 0.5 ml HBSS containing 1 mg/ml cytochrome c at  
299  $37^\circ\text{C}$ . Cytochrome c reduction at 550 nm was then measured before (Resting) and after the  
300 addition of stimuli ( $10^{-6}$  M fMLF or 100 nM PMA) to the cells. Optical Density was recorded  
301 with a spectrophotometer at 550 nm during 15 min. Superoxide dismutase (SOD) (2.5 Units)  
302 was used in each experiment to inhibit cytochrome c reduction ensuring superoxide  
303 production. The quantification of superoxide anions was calculated using  
304  $\epsilon = 21.1 \text{ cm}^2 \text{ mol}^{-1} \text{ min}^{-1}$ . Total superoxide anion production was calculated and expressed as  
305 “nanomoles/15min/1 million cells” or as the initial rate “nanomoles/min/1 million cells”.

306

307 *Measurement of luminol-amplified chemiluminescence*

308

309 Monocytes ( $5 \times 10^5$ ) were suspended in 0.5 ml HBSS containing 10  $\mu\text{M}$  luminol at  $37^\circ\text{C}$ .  
310 ROS production was then measured before (Resting) and after the addition of stimuli ( $10^{-6}$  M  
311 fMLF or 100 nM PMA) to the cells. Luminol-amplified chemiluminescence was recorded  
312 with a luminometer (Berthold-Biolumat LB937) (36,37).

313

## 314 *SDS-PAGE and Western Blotting*

315

316 Gel electrophoresis and protein transfer to nitrocellulose membranes were performed with  
317 classical techniques (31). Nitrocellulose membranes were blocked with 5% non fat dry milk  
318 in borate-buffered saline, pH 8.4 (100 mM boric acid, 25 mM borax and 75 mM NaCl) for 1 h  
319 at room temperature and then incubated with 1:1000 mouse monoclonal anti- gp91phox  
320 antibody, -p22phox or -PAT1 antibody overnight. The membranes were then washed  
321 extensively and incubated with horseradish peroxidase-conjugated 1:5000 anti-mouse IgG for  
322 1 h at room temperature. Blots were visualized by using enhanced chemiluminescence  
323 Western blotting reagents (Amersham Pharmacia).

324

## 325 *Statistical analysis*

326

327 Data were analysed with the GraphPad Prism 5 software. Differences between groups were  
328 analysed by the One-way ANOVA test with Tukey's Multiple Comparison post-test. \* $p < 0.05$ ,  
329 \*\* $p < 0.01$ , and \*\*\* $p < 0.001$  values were considered as significant.

330

## 331 **Results**

332

### 333 *Identification of PAT1 as a p22phox-interacting protein*

334 To identify potential p22phox-interacting proteins, we performed a yeast two-hybrid screen of  
335 a human spleen cDNA library using the cytosolic C-terminal region of p22phox (residues  
336 132-195) (Fig. 1A). This construct does not induce background as manifested by the absence  
337 of transactivation of the two reporter genes, His 3 and LacZ. Among the histidine and beta-  
338 galactosidase positive clones, one clone has passed all the non specific interaction controls: in

339 the absence of the bait, the pACT2 isolated from this clone does not induce the transactivation  
340 of both reporter genes (Fig. 1B). This clone contained a 886 kb insert whose sequence  
341 matched the human PAT1 sequence encoding amino acids 1 to 277 (Fig. S1). To confirm the  
342 p22phox/PAT1 interaction detected in the two-hybrid experiments, we performed a GST pull-  
343 down assay using purified recombinant human PAT1a (99 % identical to PAT1) and GST-  
344 p22phox (residues 132-195). Results obtained by western blots and protein quantification  
345 show that GST-p22phox was able to pull-down PAT1a while GST alone was not (Fig. 1C-left  
346 and right). This interaction was also confirmed by an overlay assay, western blots and  
347 quantification of the proteins (Fig. 1D-left and right). To investigate if PAT1 also associates  
348 with gp91phox or not, GST-Pull down assay was also performed using the GST fusion  
349 protein containing the cytoplasmic C-terminal domain of gp91phox (amino acids (aa) 291-  
350 570). Results show that GST-gp91phox-Cter was not able to interact with PAT1 (Fig. S2).  
351 These results demonstrate the specific interaction between PAT1 and p22phox, but also show  
352 a direct association without the need for any other protein or agent.

353 To study the PAT1-p22phox interaction in intact cells, we used the COSphox cell line system  
354 i.e. COS cells transfected with all the components of the phagocytes NADPH oxidase (33,34).  
355 Transfection of COSphox cells with HA-tagged PAT1-pRK5 plasmid resulted in a clear  
356 overexpression of PAT1 as shown by western blots and protein quantifications data (Fig. 2A-  
357 left and right). Immunoprecipitation of cytochrome b558 using an anti-gp91phox or anti-  
358 p22phox antibody showed that PAT1 co-immunoprecipitated with the complex (Fig. 2B),  
359 while the use of control IgG did not demonstrate the presence of PAT1. These results clearly  
360 demonstrate that PAT1 interacts with p22phox in intact cells using a reconstituted cell system.

361

362 *PAT1 is expressed in human neutrophils, monocytes and lymphocytes and it colocalizes with*  
363 *p22phox*

364 The expression of PAT1 has been observed in some cells such as epithelial cells (23-26), but  
365 its presence in human neutrophils and other leukocytes had not been yet investigated. To look  
366 for the expression of PAT1 in these human blood cells, the total RNA's were extracted from  
367 highly purified neutrophils, monocytes and lymphocytes and PAT1 mRNA expression was  
368 analysed using specific primers and RT-qPCR cDNA quantification. Results show that PAT1  
369 mRNA was expressed in the three types of blood cells at comparable levels (Fig. 3A). To  
370 validate the expression of PAT1 protein, equal amounts of cells were analysed by SDS-PAGE  
371 and Western Blot using two different specific antibodies against human PAT1. Results with  
372 both antibodies show that PAT1 protein is expressed in the three cell types (Fig. 3B).  
373 Confocal microscopy analysis confirmed PAT1 expression in human neutrophils (Fig. 3C-  
374 PAT1). To investigate PAT1-p22phox interaction in neutrophils, we first explored the  
375 possibility of colocalization in intact neutrophils using confocal microscopy. Interestingly, in  
376 resting neutrophils, PAT1 showed a cytoplasmic, nuclear and perinuclear localisation while  
377 p22phox showed granular and perinuclear localisation (Fig. 3C). In resting neutrophils, PAT1  
378 colocalised partially with p22phox especially in the peri-nuclear region. We found that, upon  
379 stimulation with fMLF ( $10^{-6}$  M) or PMA (100 ng/ml), the distribution of PAT1 is modified, it  
380 was mainly recruited at the plasma membrane where it displays colocalisation with p22phox  
381 (Fig. 3C). A PAT1-p22phox colocalization was also clearly found in resting and PMA-  
382 stimulated monocytes (Fig. S3). These results suggest that translocation of the PAT1 to the  
383 plasma membrane takes place following stimulation. To confirm this result, cytoplasmic,  
384 nuclear, cytosolic and membrane extracts were prepared from resting and stimulated  
385 neutrophils. Protein analysis shows that in resting cells PAT1 is mainly located in the nucleus  
386 and in cytosol at a lower extent, and that stimulation of neutrophils induced a decrease of the

387 PAT1 level in the nuclear fraction with an increase in the cytosolic or cytoplasmic fractions as  
388 well as a translocation to the membrane (Fig. 3D and 3E).

389

#### 390 *PAT1 interacts with cytochrome b558 in human neutrophils*

391 To further investigate the PAT1/p22phox interaction in human neutrophils, we used a co-  
392 immunoprecipitation assay from intact neutrophils. Cell lysates from resting or fMLF- or  
393 PMA-stimulated neutrophils were immunoprecipitated with anti-cytochrome b558 7D5-  
394 antibody which recognizes extracellular “gp91phox/p22phox complex” also known as the  
395 cytochrome b558, without interfering with intracellular interactions. Results show that PAT1  
396 was detected in the cytochrome b558 complex containing gp91phox and p22phox of resting  
397 and stimulated neutrophils, while it was less detected in beads with control IgG isotype (Fig.  
398 4A). The PAT1/cytochrome b558 interaction was further confirmed by co-  
399 immunoprecipitation assay using the specific NOX2 antibody, in COSphox cells transfected  
400 with the PAT1 and the FPR (Formyl Peptide Receptor) plasmids (Fig. 4B), while the use of  
401 control IgG did not demonstrate the presence of PAT1. Protein quantification analysis of  
402 several western blots showed that fMLF induced a significant increase of PAT1/cytochrome  
403 b558 interaction in both cells, while PMA was less effective.

404

#### 405 *PAT1 promotes superoxide anion production in intact cells*

406 We further investigated the functional effects of the PAT1-p22phox interaction in living cells  
407 overexpressing PAT1. Because neutrophils have a short life span and are resistant to  
408 transfection procedures, we used alternative cells for PAT1 over-expression or PAT1 knock  
409 down. Firstly, we used COSphox cell lines which are transfected with either the fMLF  
410 receptor (FPR) or the C5a receptor (34), with or without PAT1 plasmid. Transfection of

411 PAT1 in COSphox cells, clearly increased fMLF- and C5a-induced ROS production (Fig. 5A  
412 and 5B). Interestingly, constitutive and PMA-induced ROS productions were only slightly  
413 enhanced (Fig. 5C).

414 Secondly, we used the siRNA approach to inhibit endogeneous PAT1 expression in  
415 monocytes. Western blots and quantification data show that monocytes-PAT1 protein level  
416 was down regulated by PAT1 siRNA but not by scramble control siRNA (Fig. 6A-left and  
417 right). We used the cytochrome c reduction assay to monitor precisely superoxide anion  
418 production and NADPH oxidase activation. Interestingly, inhibition of PAT1 expression  
419 resulted in total superoxide anion production (15 min period) inhibition in fMLF- and PMA-  
420 stimulated neutrophils (Fig.6B), however the initial rate of superoxide anion production was  
421 not affected (Fig. 6C). These results were further confirmed by luminol-amplified  
422 chemiluminescence technique (Fig. S4). Furthermore, we over-expressed PAT1 in human  
423 monocytes using an Amaxa transfection system. As shown in Fig. 6D, transfection of human  
424 monocytes with a plasmid encoding PAT1a resulted in overexpression of the protein. GFP  
425 expression was also used to check the transfection efficiency of monocytes (data not shown).  
426 Interestingly, monocytes overexpressing PAT1 showed enhanced superoxide anions  
427 production as measured by the cytochrome c reduction assay (Fig.6E) as well as ROS  
428 production as measured by luminol-amplified chemiluminescence of fMLF- and PMA-  
429 stimulated monocytes (data not shown).

430

## 431 **Discussion**

432 ROS production by the phagocyte NADPH oxidase NOX2 is an essential process for host  
433 defense against pathogens (3-5). However, excessive NADPH oxidase activation is believed

434 to be involved in inflammatory reactions (38,39). Tight regulation of NADPH oxidase  
435 activation is important to ensure that ROS are produced only when and where required.  
436 Several mechanisms, such as protein phosphorylation, GTPase activation and protein/protein  
437 interactions regulate NADPH oxidase activation (8-12). Results presented in this study  
438 uncover a novel mechanism of regulating NOX2 and ROS production based on  
439 p22phox/PAT1 interaction. We used different approaches to show the interaction between  
440 p22phox and PAT1; the yeast two hybrid system, the GST pull-down assay, the overlay assay,  
441 confocal microscopy and co-immunoprecipitation techniques. Interestingly, PAT1 does not  
442 interact with the gp91phox cytosolic region suggesting that PAT1 interacts specifically with  
443 p22phox. We showed that this interaction is functional, PAT1 overexpression increased  
444 NADPH oxidase-derived ROS production in human monocytes and in the COSphox cells.  
445 Furthermore, we have shown that inhibition of PAT1 expression in human monocytes resulted  
446 in an inhibition of total superoxide anion production but not the initial rate of superoxide  
447 production. This result suggest that PAT1 is not involved in the initiation of NADPH oxidase  
448 activation but rather it is required to sustain the activation in human monocytes.

449 PAT1 mRNA is expressed in different tissues such as heart, brain, placenta, skeletal muscle,  
450 kidney and pancreas (23-26). At least three isoforms of PAT1 have been described in the  
451 literature; they are almost identical differing by only a few amino acids. These isoforms  
452 comprise PAT1 itself, ARA67 which is 99.6% identical to PAT1 and PAT1a which is 99%  
453 identical to PAT1. The sequence identified in this study is shared by the three isoforms,  
454 however the isoforms expressed in human neutrophils remain undetermined. Since the three  
455 isoforms are 99% identical, and the yeast two-hybrid-identified the common N-terminal  
456 domain as interacting with p22phox, all three isoforms could potentially interact with the  
457 p22phox cytosolic tail.

458 Interestingly, PAT1 enhances fMLF- and C5a-induced NADPH oxidase activation and to a  
459 lesser extent the PMA-induced activation. Since fMLF and C5a are physiological agonists  
460 which activate two different G-protein coupled receptors and PMA is a strong  
461 pharmacological activator of conventional PKC, these results suggest that PAT1 could play a  
462 major role in G-protein coupled receptors-mediated NADPH oxidase activation. The  
463 conventional PKC-mediated NADPH oxidase pathway may be regulated to a lesser extent by  
464 PAT1. More studies are required to try to understand this process.

465 PAT1 binds microtubules and is involved in intracellular trafficking of several proteins  
466 including  $\beta$ -amyloid precursor protein (APP) (23,24), Us11 virus protein (40), and androgen  
467 receptor (26). It is not excluded that PAT1 could play a role in p22phox production or in the  
468 trafficking of p22phox rich granules in phagocytes. We have confirmed that PAT1 binds to  
469 microtubules *in vitro* and was able to mediate p22phox binding (data not shown).  
470 Interestingly, cytochrome b558 was shown to undergo conformational changes and to bind to  
471 cytoskeleton with activated NADPH oxidase (41-43). PAT1 may facilitate the conformational  
472 changes of cytochrome b558 and its binding to cytoskeleton. Thus, PAT1 could control  
473 localization of NADPH oxidase activation in the cell.

474 P22phox expression is not restricted to phagocytes; it is expressed in several tissues and cells  
475 such as vascular smooth muscle cells, epithelial cells, endothelial cells and neurons. In  
476 addition, p22phox is associated with other NOX enzymes such as NOX1, NOX3 and NOX4  
477 (10,44). We have recently shown that p22phox could bind to NOX5 in monocyte-derived  
478 DC35. Using the yeast two-hybrid system and a vascular smooth muscle cell cDNA library,  
479 Lyle et al, (45) have identified Poldip2 protein as a partner of p22phox. Poldip2 increased  
480 NOX4 enzymatic activity in vascular smooth muscle cells and modulated cytoskeletal

481 remodeling and cell migration. Our results and those reported by Lyle et al (45), suggest that  
482 p22phox could have several partners which probably depend on p22phox tissue expression.

483 In conclusion, we have shown that PAT1 is able to bind to the region of the p22phox  
484 cytosolic tail composed of aminoacids 132 to 195 and is capable of enhancing NADPH  
485 oxidase activation *in vitro* and in intact cells. PAT1 was first identified in human cells as  
486 binding to APP and to microtubules. Here we describe a novel function of PAT1 in human  
487 phagocytic cells. Several other cells express p22phox in association with other NOX  
488 enzymes, therefore, PAT1 could be a novel regulator of superoxide anion and ROS  
489 production in these cells.

490

491 **Aknowledgements:**

492 We would like to thank Dr Mary Dinauer (Riley Hospital for Children, Indiana University  
493 School of Medicine, Indianapolis, IN, USA) for the generous gift of the p22phox plasmid, Dr  
494 Marie-Christine Lecomte (INSERM U1134) for her help on the two-hybrid system and Dr  
495 Stefan Kins (ZMBH, University of Heidelberg, Germany) for the generous gift of the PAT1a  
496 cDNA containing plasmid.

497

## References

- 498 1. Nathan, C. 200. Neutrophils and immunity: challenges and opportunities. *Nat. Rev.*  
 499 *Immunol.* 6: 173-182.  
 500
- 501 2. Witko-Sarsat, V., P. Rieu, B. Descamps-Latscha, P. Lesavre, L. Halbwachs-Mecarelli.  
 502 2000. Neutrophils: molecules, functions and pathophysiological aspects. *Lab. Invest.* 80: 617-  
 503 653.  
 504
- 505 3. Nauseef, W. M., N. Borregaard. 2014. Neutrophils at work. *Nat. Immunol.* 15: 602-  
 506 611.  
 507
- 508 4. Nauseef, W. M. 2007. How human neutrophils kill and degrade microbes: an integrated  
 509 view. *Immunol. Review.* 219: 88-102.  
 510
- 511 5. El-Benna, J., P. M. Dang, MA. Gougerot-Pocidallo, C. Elbim. 2005. Phagocyte  
 512 NADPH oxidase: a multicomponent enzyme essential for host defenses. *Arch. Immunol. Ther.*  
 513 *Exp. (Warsz)* 53: 199-206.  
 514
- 515 6. Hampton, M. B., A. J. Kettle, C. C. Winterbourn. 1998. Inside the neutrophil  
 516 phagosome: oxidants, myeloperoxidase, and bacterial killing. *Blood.* 92: 3007-3017.  
 517
- 518 7. Babior, B. M. 1999. NADPH oxidase: an update. *Blood.* 93: 1464-1476.  
 519
- 520 8. Chanock, S. J., J. El-Benna, R. M. Smith and B. M. Babior. 1994. The respiratory  
 521 burst oxidase. *J. Biol. Chem.* 269: 24519-24522.  
 522
- 523 9. Groemping, Y., and K. Rittinger. 2005. Activation and assembly of the NADPH  
 524 oxidase: a structural perspective. *Biochem. J.* 386: 401-416.  
 525
- 526 10. Nauseef, W. M. 2008. Biological roles for the NOX family NADPH oxidases. *J. Biol.*  
 527 *Chem.* 283: 16961-16965.  
 528
- 529 11. Vignais, P. V. 2002. The superoxide-generating NADPH oxidase: structural aspects  
 530 and activation mechanism. *Cell. Mol. Life. Sci.* 59: 1428-1459.  
 531
- 532 12. El-Benna, J, Dang PMC, and Gougerot-Pocidallo MA. Priming of the neutrophil  
 533 NADPH oxidase activation: role of p47phox phosphorylation and NOX2 mobilization to the  
 534 plasma membrane. *Semin Immunopathol.* 2008;30(3):279-289.  
 535
- 536 13. El-Benna, J., P. M. Dang, MA. 2009. Gougerot-Pocidallo, J. C. Marie, F. Braut-  
 537 Boucher. p47phox, the phagocyte NADPH oxidase/NOX2 organizer: structure,  
 538 phosphorylation and implication in diseases. *Exp. Mol. Med.* 41: 217-225.  
 539
- 540 14. Groemping, Y., K. Lapouge, S. J. Smerdon, K. Rittinger. 2003. Molecular basis of  
 541 phosphorylation-induced activation of the NADPH oxidase. *Cell.* 113: 343-355.  
 542
- 543 15. Dang, P. M., F. Morel, MA. Gougerot-Pocidallo, J. El Benna. 2003. Phosphorylation of  
 544 the NADPH oxidase component p67(PHOX) by ERK2 and P38MAPK: selectivity of

- 545 phosphorylated sites and existence of an intramolecular regulatory domain in the  
546 tetratricopeptide-rich region. *Biochemistry*. 42: 4520-4526.  
547
- 548 **16.** Lewis, E. M., S. Sergeant, B. Ledford, N. Stull, M. C. Dinauer, L. C. McPhail. 2010.  
549 Phosphorylation of p22phox on threonine 147 enhances NADPH oxidase activity by  
550 promoting p47phox binding. *J. Biol. Chem.* 285: 2959-2967.  
551
- 552 **17.** Paclet, M. H., S. Berthier, L. Kuhn, J. Garin, F. Morel. 2007. Regulation of phagocyte  
553 NADPH oxidase activity: identification of two cytochrome b558 activation states. *FASEB. J.*  
554 21: 1244-1255.  
555
- 556 **18.** Raad, H., M. H. Paclet, T. Boussetta, Y. Kroviarski, F. Morel, M. T. Quinn, M-A.  
557 Gougerot-Pocidallo, P. M. Dang, J. El-Benna. 2009. Regulation of the phagocyte NADPH  
558 oxidase activity: phosphorylation of gp91phox/NOX2 by protein kinase C enhances its  
559 diaphorase activity and binding to Rac2, p67phox, and p47phox. *FASEB. J.* 23: 1011-1022.  
560
- 561 **19.** Leto, T. L., A. G. Adams, I. 1994. de Mendez. Assembly of the phagocyte NADPH  
562 oxidase: binding of Src homology 3 domains to proline-rich targets. *Proc. Natl. Acad. Sci.*  
563 *USA.* 91: 10650-10654.  
564
- 565 **20.** Sumimoto, H., K. Hata, K. Mizuki, T. Ito, Y. Kage, Y. Sakaki, Y. Fukumaki, M.  
566 Nakamura M, K. Takeshige. 1996. Assembly and activation of the phagocyte NADPH  
567 oxidase. Specific interaction of the N-terminal Src homology 3 domain of p47phox with  
568 p22phox is required for activation of the NADPH oxidase. *J. Biol. Chem.* 271: 22152-22158.  
569
- 570 **21.** Fontayne, A., P. M. Dang, MA. Gougerot-Pocidallo, J. El-Benna. 2002.  
571 Phosphorylation of p47phox sites by PKC alpha, beta II, delta, and zeta: effect on binding to  
572 p22phox and on NADPH oxidase activation. *Biochemistry*. 41: 7743-7750.  
573
- 574 **22.** Dinauer, M. C., E. A. Pierce, R. W. Erickson, T. J. Muhlebach, H. Messner, S. H.  
575 Orkin, R. A. Seger, J. T. Curnutte. 1991. Point mutation in the cytoplasmic domain of the  
576 neutrophil p22-phox cytochrome b subunit is associated with a nonfunctional NADPH  
577 oxidase and chronic granulomatous disease. *Proc. Natl. Acad. Sci. USA.* 88: 11231-11235.  
578
- 579 **23.** Zheng, P., J. Eastman, S. Vande Pol, S. W. Pimplikar. 1998. PAT1, a microtubule-  
580 interacting protein, recognizes the basolateral sorting signal of amyloid precursor protein.  
581 *Proc. Natl. Acad. Sci. U S A.* 95: 14745-14750.  
582
- 583 **24.** Kuan, Y.H., T. Gruebl, P. Soba, S. Eggert, I. Nestic, S. Back, J. Kirsch, K. Beyreuther,  
584 S. Kins. 2006. PAT1a modulates intracellular transport and processing of amyloid precursor  
585 protein (APP), APLP1, and APLP2. *J. Biol. Chem.* 281: 40114-40123.  
586
- 587 **25.** Gao, Y., S. W. Pimplikar. 2001. The gamma-secretase-cleaved C-terminal fragment of  
588 amyloid precursor protein mediates signaling to the nucleus. *Proc. Natl. Acad. Sci. USA.* 98:  
589 14979-14984.  
590
- 591 **26.** Zhang, Y., Y. Yang, S. Yeh, C. Chang. 2004. ARA67/PAT1 functions as a repressor to  
592 suppress androgen receptor transactivation. *Mol. Cell. Biol.* 24: 1044-1057.  
593

- 594 **27.** Van Aelst, L., M. Barr, S. Marcus, A. Polverino, M. Wigler. 1993. Complex formation  
595 between RAS and RAF and other protein kinases. *Proc. Natl. Acad. Sci. USA.* 90: 6213-6217.  
596
- 597 **28.** Rotter, B., Y. Kroviarski, G. Nicolas, D. Dhermy, M. C. Lecomte. 2004. AlphaII-  
598 spectrin is an in vitro target for caspase-2, and its cleavage is regulated by calmodulin  
599 binding. *Biochem. J.* 378: 161-168.  
600
- 601 **29.** Dang, P. M., A. R. Cross, B. M. Babior. 2001. Assembly of the neutrophil respiratory  
602 burst oxidase: a direct interaction between p67PHOX and cytochrome b558. *Proc. Natl. Acad.*  
603 *Sci. USA.* 98: 3001-3005.  
604
- 605 **30.** Nauseef, W.M. 2014. Isolation of human neutrophils from venous blood. *Methods Mol.*  
606 *Biol.* 1124:13-18.  
607
- 608 **31.** Belambri, S.A., Dang, P.M., El-Benna, J. 2014. Evaluation of p47phox  
609 phosphorylation in human neutrophils using phospho-specific antibodies. *Methods Mol. Biol.*  
610 1124:427-433.  
611
- 612 **32.** Tamassia, N., Cassatella, M.A., Bazzoni, F. 2014. Fast and accurate quantitative  
613 analysis of cytokine gene expression in human neutrophils. *Methods Mol. Biol.* 1124:451-67.  
614
- 615 **33.** Price, M. O., L. C. McPhail, J. D. Lambeth, C. H. Han, U. G. Knaus, M. C. Dinauer.  
616 2002. Creation of a genetic system for analysis of the phagocyte respiratory burst: high-level  
617 reconstitution of the NADPH oxidase in a nonhematopoietic system. *Blood.* 99: 2653-2661.  
618
- 619 **34.** He, R., M. Nanamori, H. Sang, H. Yin, M. C. Dinauer, R. D. Ye R. 2004.  
620 Reconstitution of chemotactic peptide-induced nicotinamide adenine dinucleotide phosphate  
621 (reduced) oxidase activation in transgenic COS-phox cells. *J. Immunol.* 173: 7462-7470.  
622
- 623 **35.** Marzaioli, V., M. Hurtado-Nedelec, C. Pintard, A. Tlili, J. C. Marie, R. C. Monteiro,  
624 MA. Gougerot-Pocidalò, P. M. Dang, J. El-Benna. 2017. NOX5 and p22phox are 2 novel  
625 regulators of human monocytic differentiation into dendritic cells. *Blood.* 130: 1734-1745.  
626
- 627 **36.** Dahlgren, C., Karlsson, A. 1999. Respiratory burst in human neutrophils. *J. Immunol.*  
628 *Methods.* 232:3-14.  
629
- 630 **37.** Bedouhène, S., Moulti-Mati, F., Hurtado-Nedelec, M., Dang, P.M., El-Benna, J. 2017.  
631 Luminol-amplified chemiluminescence detects mainly superoxide anion produced by human  
632 neutrophils. *Am. J. Blood. Res.* 7:41-48.  
633
- 634 **38.** Babior, B. M. 2000. Phagocytes and oxidative stress. *Am. J. Med.* 109: 33-44.  
635
- 636 **39.** El Benna, J., P. M. C. Dang, M. Hurtado-Nedelec, J. C. Marie, M-A. Gougerot-  
637 Pocidalò. 2016. Priming of the neutrophil respiratory burst : Role in host defense and  
638 inflammation. *Imm. Rev.* 273: 180-193.  
639
- 640 **40.** Benboudjema, L., M. Mulvey, Y. Gao, S. W. Pimplikar, I. Mohr. 2003. Association of  
641 the herpes simplex virus type 1 Us11 gene product with the cellular kinesin light-chain-related  
642 protein PAT1 results in the redistribution of both polypeptides. *J. Virol.* 77: 9192-9203.  
643

- 644 **41.** Woodman, RC, J. M. Ruedi, A. J. Jesaitis, N. Okamura, M. T. Quinn, R. M. Smith, J.  
645 T. Curnutte, B. M. Babior. 1991. Respiratory burst oxidase and three of four oxidase-related  
646 polypeptides are associated with the cytoskeleton of human neutrophils. *J. Clin. Invest.*  
647 1991;87(4):1345-1351.  
648
- 649 **42.** Nauseef, W. M., B. D. Volpp, S. McCormick, K. G. Leidal, R. A. Clark. 1991.  
650 Assembly of the neutrophil respiratory burst oxidase. Protein kinase C promotes cytoskeletal  
651 and membrane association of cytosolic oxidase components. *J. Biol. Chem.* 266: 5911-5917.  
652
- 653 **43.** El Benna, J., J. M. Ruedi, B. M. Babior. 1994. Cytosolic guanine nucleotide-binding  
654 protein Rac2 operates in vivo as a component of the neutrophil respiratory burst oxidase.  
655 Transfer of Rac2 and the cytosolic oxidase components p47phox and p67phox to the  
656 submembranous actin cytoskeleton during oxidase activation. *J. Biol. Chem.* 269: 6729-6734.  
657
- 658 **44.** Bedard, K., K. H. Krause. 2007. The NOX family of ROS-generating NADPH  
659 oxidases: physiology and pathophysiology. *Physiol. Rev.* 87: 245-313.  
660
- 661 **45.** Lyle, A. N., N. N. Deshpande, Y. Taniyama, B. Seidel-Rogol, L. Pounkova, P. Du, C;  
662 Papaharalambus, B. Lassegue, K. K. Griendling. 2009. Poldip2, a novel regulator of Nox4  
663 and cytoskeletal integrity in vascular smooth muscle cells. *Circ. Res.* 105: 249-259.  
664

665 **Footnotes**

666

667 This work was supported by grants from Agence Nationale de la Recherche (ANR), Arthritis  
668 Fondation Courtin, VLM (Vaincre La Mucoviscidose), INSERM, CNRS, Labex Inflammex and  
669 University Denis-Diderot Paris7.

670

671 \*Yvonne O'Dowd and Riad Arabi Derkawi contributed equally to this work.

672

673 **Authors contributions:** RAD and YO'D designed and performed experiments, analysed  
674 data, and wrote the manuscript; NC, LR, TB, HR, VM and CP performed experiments and  
675 analysed data; MF, YK and SAB contributed to the experiments and analysed data; PMCD,  
676 RY, MAGP and JEB supervised the project and co-wrote the manuscript.

677

678 **Corresponding authors:** Jamel El-Benna, INSERM U1149, Faculté de Médecine Xavier  
679 Bichat, 16 rue Henri Huchard, Paris F-75018, e-mails: [jamel.elbenna@inserm.fr](mailto:jamel.elbenna@inserm.fr), Tel: 33 1 57  
680 27 77 23 ; Fax: 33 1 57 27 74 71.

681

682

683 The online version of this article contains supplemental material.

684

685

686 **Figure Legends**

687

688 **Figure 1. Schematic representation of p22phox cytosolic tail and its interaction with**689 **PAT1 in the yeast two-hybrid system, in the GST pull-down assay and overlay assay. (A)**

690 Human p22phox is a transmembrane protein with two transmembrane domains and a long

691 cytosolic carboxy terminal sequence predicted from amino acid 132 to 195. (B) Summary of

692 results obtained from the two hybrid system. The p22phox cytosolic C-terminal region (132-

693 195) was fused to the LexA protein (pLex10 vector), as bait to screen a human spleen cDNA

694 library in pACT2 vector. The histidine and  $\beta$ -galactosidase positive clone was designed as (+)

695 and negative result was designed as (-). Specificity of p22phox (132-195)/PAT1 interaction:

696 the pACT2-PAT1 clone was used to verify its interaction with the empty pLex vector and

697 with pLex10-p22phox(132-195). The histidine and beta-galactosidase positive clones were

698 designed as (+) and negative result was designed as (-). (C) Recombinant human PAT1

699 (PAT1) was incubated with GST-p22phox(132-195) or with GST protein and then with

700 Glutathione (GSH)-agarose beads for 1h. After this incubation, the beads were washed three

701 times and proteins were analyzed by SDS-PAGE and Western Blot using anti-GST or

702 polyclonal anti-PAT1 antibodies (left). Bound PAT1 and GST were quantified using Image J

703 1.43u software (Wayne Rasband, National Institute of Health, USA) and their ratio was

704 calculated and the values are expressed as means  $\pm$  SEM of 3 independent experiments. (\*  $p <$ 

705 0.05 GST-p22phox as compared to GST alone) (right). (D) Recombinant human PAT1 was

706 analyzed by SDS-PAGE and overlay assay using GST alone or GST-p22phox and the

707 proteins were detected using using anti-GST antibody (left). Bound PAT1 were quantified

708 using Image J 1.43u software and the values are expressed as means  $\pm$  SEM of 3 independent709 experiments. (\* $p <$  0.05 GST-p22phox as compared to GST alone) (right).

710

711 **Figure 2. Over-expression of PAT1 in COSphox and co-immunoprecipitation with**  
712 **p22phox and gp91phox.** (A) COSphox cells were transfected with a plasmid expressing  
713 PAT1a (pRK5-PAT1a-HA) or control plasmid without PAT1a and lysed in lysis buffer.  
714 Proteins were analyzed by SDS-PAGE and Western blot with anti-HA, anti-PAT1, anti-  
715 p22phox and anti-p47phox antibodies (left). PAT1 and p22phox were quantified using Image  
716 J 1.43u software and their ratio was calculated and the values are expressed as means  $\pm$  SEM  
717 of 3 independent experiments. (\*  $p < 0.05$  pRK5-PAT1 as compared to pRK5) (right). (B)  
718 Proteins were immunoprecipitated from resting COSphox cells lysates with anti-gp91phox or  
719 anti-p22phox antibody or control IgG and analyzed by SDS-PAGE and western blot with anti-  
720 PAT1a, anti-p22phox or anti-gp91phox antibodies. IP: immunoprecipitation; I.B: immunoblot  
721 (left). Bound and total PAT1 were quantified using Image J 1.43u software and their ratio was  
722 calculated and the values are expressed as means  $\pm$  SEM of 3 independent experiments. (\*  $p <$   
723  $0.05$  anti-gp91phox and anti-p22phox as compared to IgG) (right).

724

725 **Figure 3. Expression of PAT1 in human neutrophils, monocytes and lymphocytes and**  
726 **subcellular localization in neutrophils.** (A) PAT1 mRNA expression: Freshly isolated  
727 neutrophils, lymphocytes and monocytes were used to purify mRNA. 1 $\mu$ g of mRNA was  
728 retrotranscribed into cDNA which was quantified by Real Time PCR using specific primers  
729 amplifying common regions of the PAT1 isoforms. Arbitrary units were attributed based on  
730  $E^{\Delta CT}$  calculation (mean  $\pm$  SEM, n=4). (B) PAT1 protein expression: Recombinant human  
731 PAT1 (rhPAT1) (5 ng) and resting human neutrophils, monocytes and lymphocytes were  
732 lysed ( $1 \times 10^6$  cells) and were analyzed by SDS-PAGE and western blot with a polyclonal or a  
733 monoclonal anti-PAT1 antibody. (C) Neutrophils in the resting state or treated with fMLF  
734 ( $10^{-6}$  M) or PMA (100 ng/ml), were fixed and permeabilized as described in the “Methods”  
735 section. Cells were incubated with a rabbit anti-p22phox antibody and a mouse anti-PAT1

736 antibody followed by incubation with Alexa Fluor 488-(green) conjugated goat anti-rabbit and  
737 Alexa Fluor 568 (red) conjugated goat anti-mouse. Nuclei were stained with TO-PRO-3.  
738 Stained cells were examined with a confocal microscope and the images were analyzed. The  
739 overlap of PAT1 and p22phox is clearly seen as the white signal (arbitrary color) in the  
740 merged image and is enriched in the perinuclear region of resting neutrophils and at the  
741 membrane periphery in the activated cells. (D) Neutrophils in the resting state or treated with  
742 fMLF ( $10^{-6}$  M) or PMA (100 ng/ml), were lysed, cytoplasm and nuclei were prepared.  
743 Proteins were analyzed by SDS-PAGE and western blot with anti-PAT1, anti-Actin and anti-  
744 histone antibodies. (E) Neutrophils in the resting state or treated with fMLF ( $10^{-6}$  M) or PMA  
745 (100 ng/ml), were lysed. Cytosol and membranes were prepared. Proteins were analyzed by  
746 SDS-PAGE and western blot with anti-PAT1, anti-p22phox and anti-p47phox antibodies. (F)  
747 Membrane PAT1 and p22phox were quantified using Image J 1.43u software and their ratio  
748 was calculated and the values are expressed as means  $\pm$  SEM of 3 independent experiments.  
749 (\*  $p < 0.05$  fMLF and PMA as compared to Resting cels (Rest.)) (right).

750

751 **Figure 4. Co-immunoprecipitation of PAT1 with the cytochrome b558 in resting and**  
752 **activated neutrophils and COSphox cells.** (A) Neutrophils in the resting state or treated  
753 with fMLF ( $10^{-6}$  M) or PMA (100 ng/ml), were lysed. Cytochrome b558 was  
754 immunoprecipitated using the 7D5 antibody (+). Control IgG was used as control (-). The  
755 beads were washed and proteins denaturated and analyzed by SDS-PAGE and Western Blot  
756 using an anti-PAT1 or an anti-gp91phox or an anti-p22phox antibody (left). Bound and total  
757 PAT1 were quantified using Image J 1.43u software (Wayne Rasband, National Institute of  
758 Health, USA) and their ratio was calculated and the values are expressed as means  $\pm$  SEM of  
759 3 independent experiments. (\*  $p < 0.05$  fMLF and PMA compared to resting cells (REST.))  
760 (right). (B) The same experiment was performed with the COSphox cells transfected with the

761 FPR and PAT1 plasmids (left). (\*  $p < 0.05$  fMLF and PMA compared to resting cells (REST.)  
762 (right).

763

764 **Figure 5. Over-expression of PAT1 in COSphox cells enhanced ROS production.**

765 COSphox cells were transfected with hFPR1, or hC5aR and the PAT1a expression constructs  
766 (PAT1a) or the empty vector (Control) and stimulated with fMLF (1  $\mu$ M), C5a (100 ng/ml) or  
767 PMA (200 ng/ml). ROS production was measured using isoluminol-amplified  
768 chemiluminescence (Chemilum.) in fMLF (A)-, C5a (B)- and PMA (C)-stimulated cells and  
769 in non stimulated (NS-) conditions. An example of each condition is shown in the left panel.  
770 Integrated chemiluminescence (Chemilum.) (area under thr curve) of 5 experiments was  
771 quantified in counts per second (cps), Mean $\pm$ SEM were calculated and presented in the right  
772 panels. The data were analyzed by 2 way ANOVA using GraphPad Prism 5 software and  
773 shown as Mean $\pm$ SEM from four independent experiments. \*  $P < 0.05$ .

774

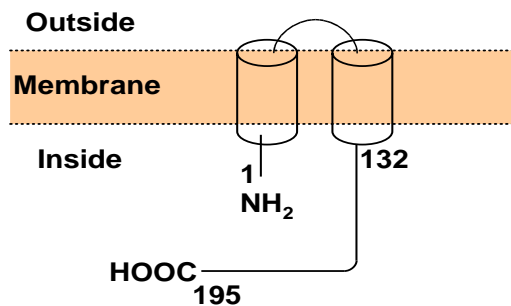
775 **Figure 6. Effect of inhibition of PAT1 expression and over-expression on human**

776 **monocytes ROS production.** (A) Human monocytes were freshly prepared and transfected  
777 with either scramble primers (Scr) or siRNA-PAT1 (si-PAT1) primers for 48h. Proteins were  
778 analyzed by SDS-PAGE and western blot with anti-PAT1 and anti-Actin antibodies (left).  
779 PAT1 and actin bands were quantified using Image J 1.43u software (Wayne Rasband,  
780 National Institute of Health, USA) and their ratio was calculated and the values are expressed  
781 as means  $\pm$  SEM of 3 independent experiments. (\*  $p < 0.05$  si-PAT1 compared to Scr) (right).  
782 Superoxide anion production was measured using the cytochrome c reduction assay at 550 nm  
783 by fMLF (10<sup>-6</sup> M)- and PMA (100 ng/ml)-stimulated cells treated with scramble and si-PAT1-  
784 RNA. Total superoxide anion production was calculated and expressed as  
785 “nanomoles/15min/1 million cells” (B) or as the initial rate “nanomoles/min/1 million cells”

786 (C) as total (\*  $p < 0.05$  si-PAT1 compared to Scr). (D) Human monocytes were freshly  
787 prepared and transfected with either a plasmid expressing PAT1a (pcDNA3.1-PAT1a)  
788 (pcDNA-PAT1) or with an empty pcDNA3.1 plasmid (pcDNA). Proteins were analyzed by  
789 SDS-PAGE and western blot with anti-PAT1 and anti-Actin antibodies and quantification  
790 analysis. (E) Superoxide anion production was measured using the cytochrome c reduction  
791 assay at 550 nm by Resting (REST.), fMLF ( $10^{-6}$  M)- and PMA (100 ng/ml)-stimulated cells.  
792 Superoxide anions production was calculated and expressed as the total nanomoles/15min/1  
793 million cells (\*  $p < 0.05$  pcDNA-PAT1 compared to pcDNA).

**Figure 1** (Arabi-Derkawi et al.)

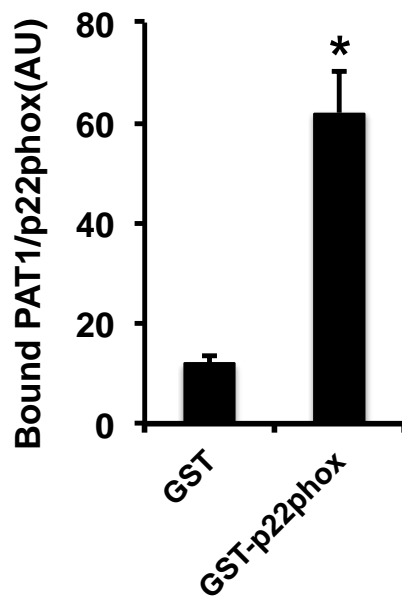
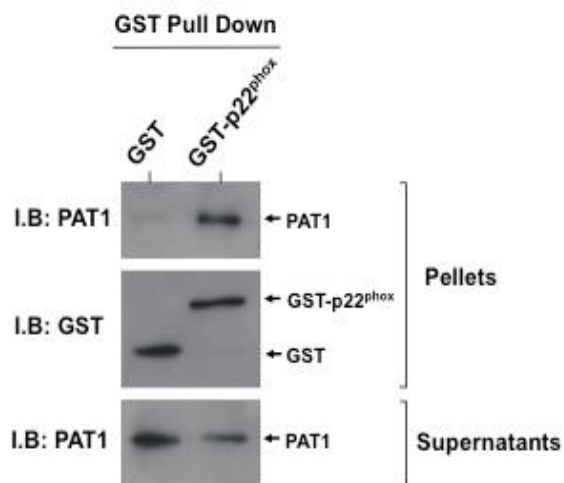
**A**



**B**

	bGal	His	pACT2-empty	pACT2-PAT1
pLex10-empty:	-	-	-	-
pLex10-p22phox:	+	+	-	+
	pACT2 Library		bGalactosidase	

**C**



**D**

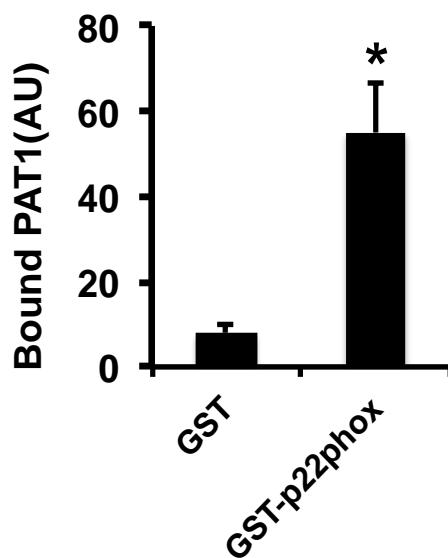
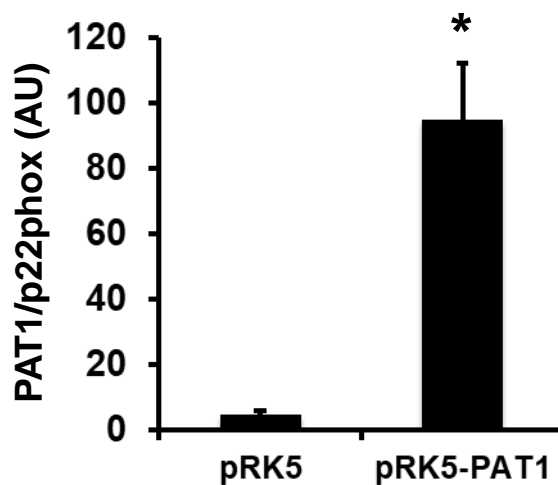
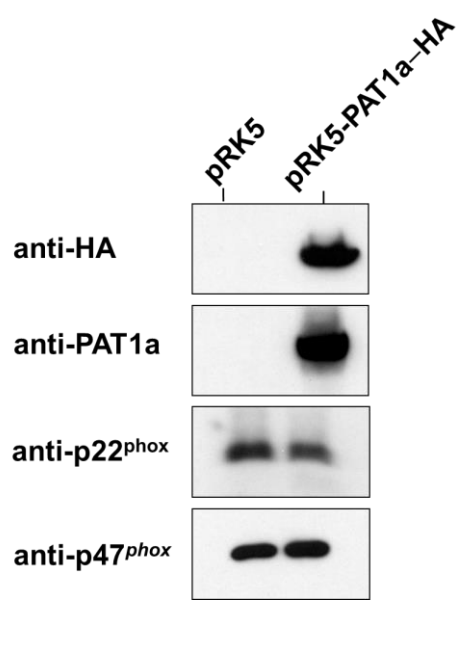
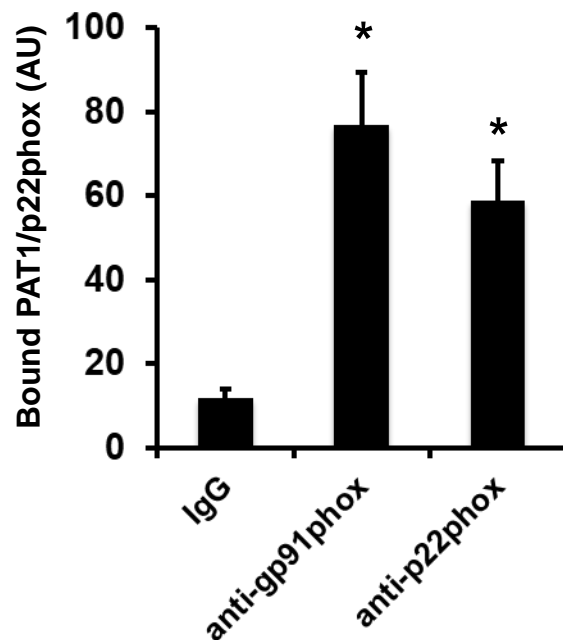
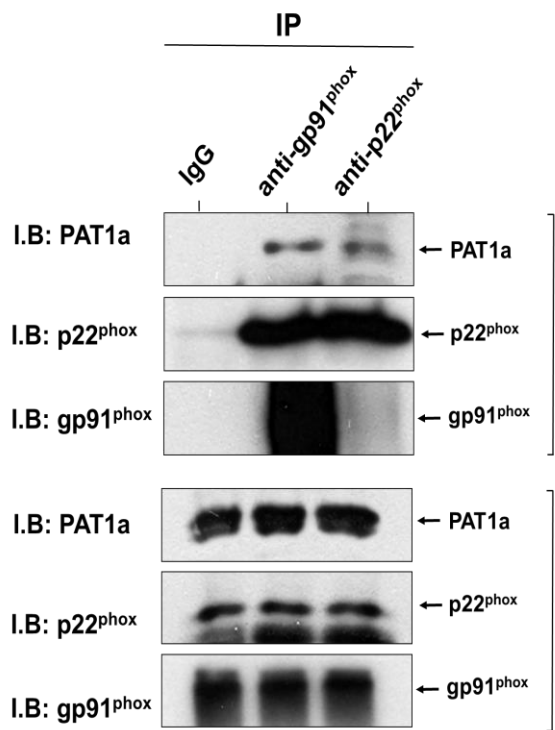


Figure 2 (Arabi-Derkawi et al.)

A



B



**Figure 3** (Arabi-Derkawi et al.)

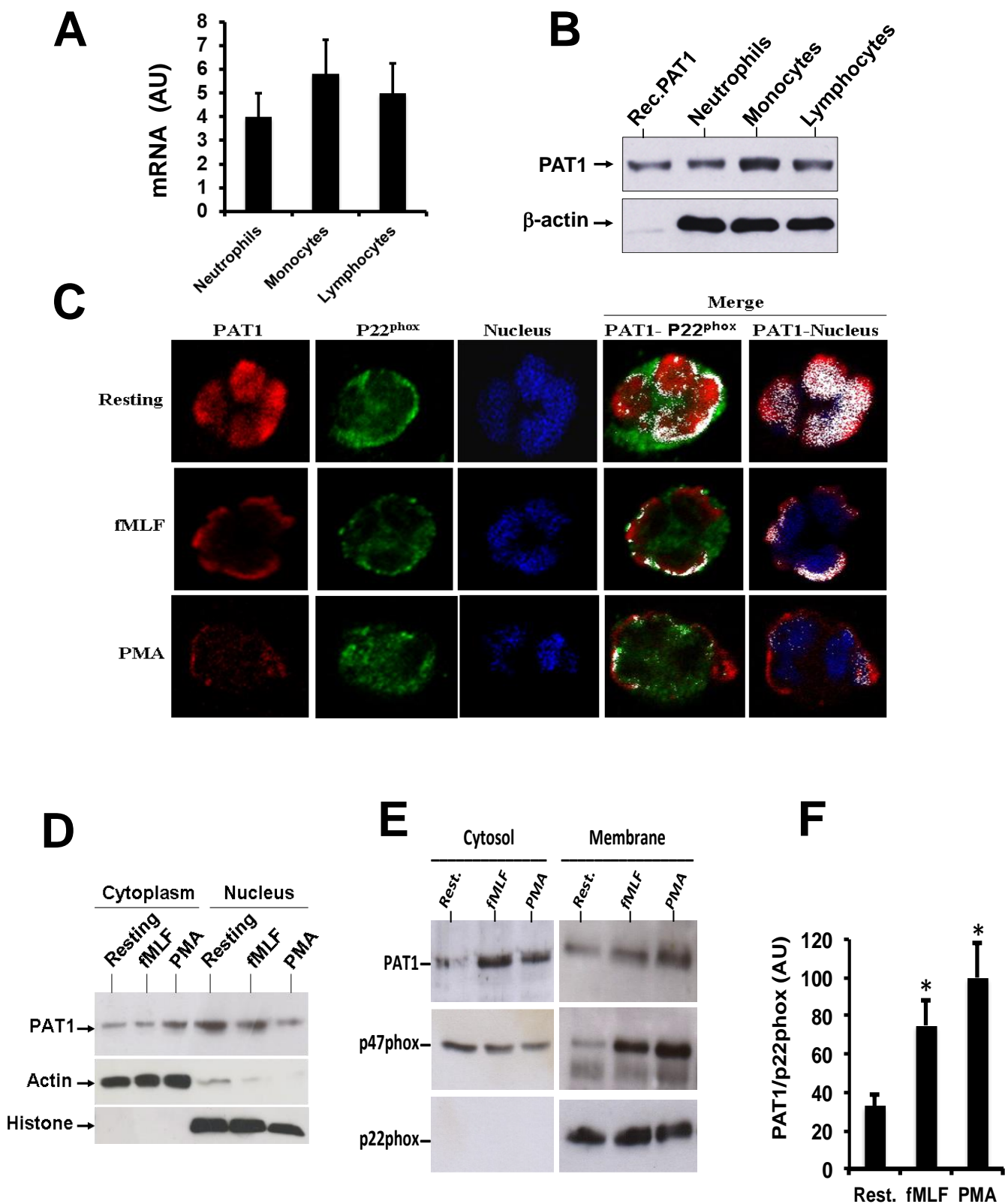
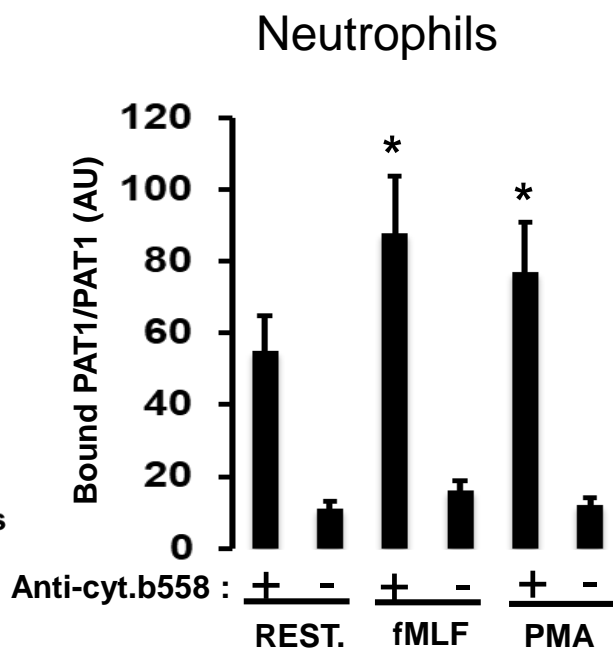
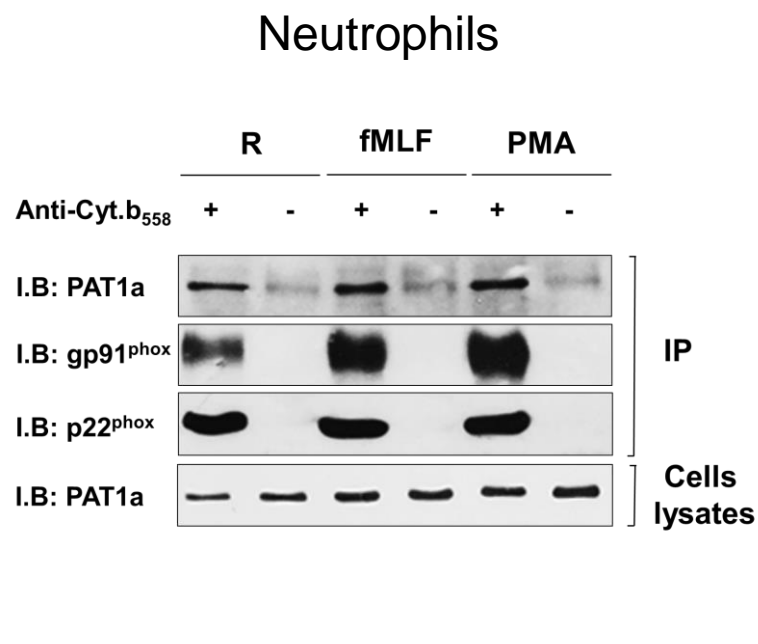


**Figure 4** (Arabi-Derkawi et al.)

**A**



**B**

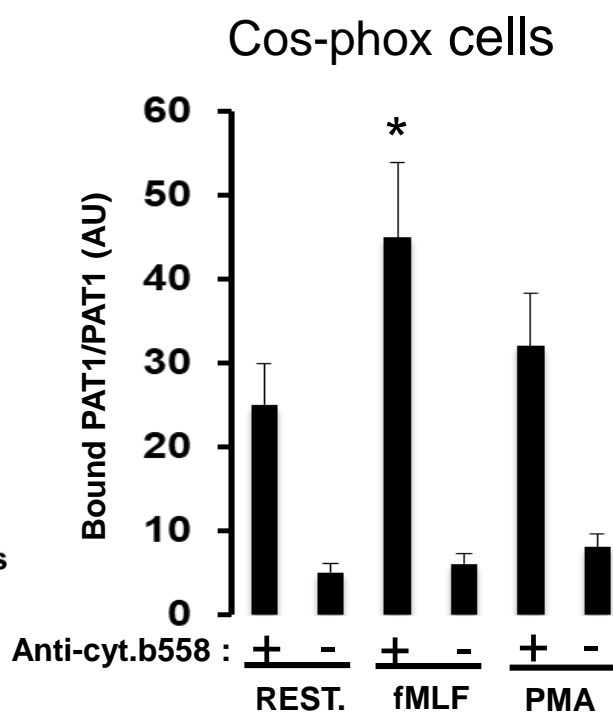
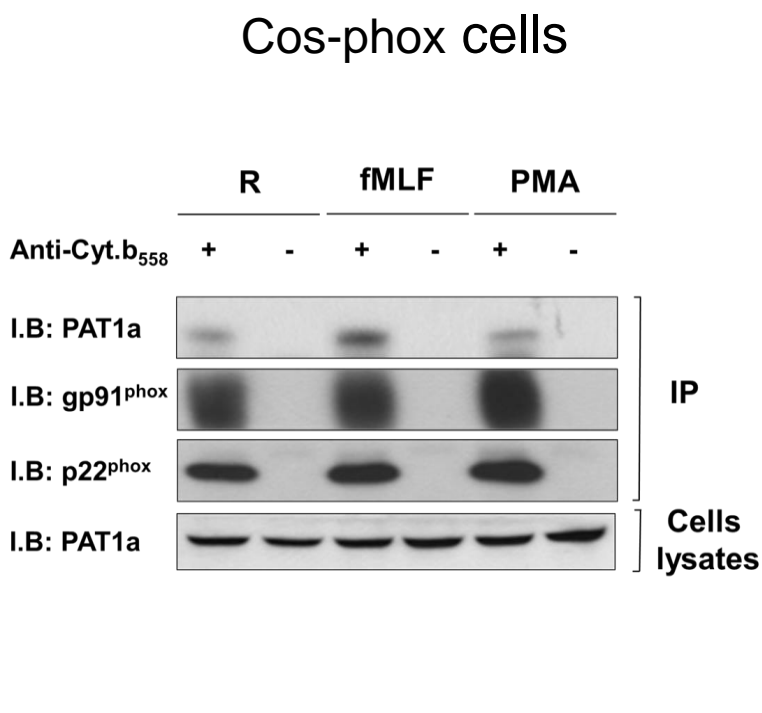


**Figure 5 (Arabi-Derkawi et al.)**

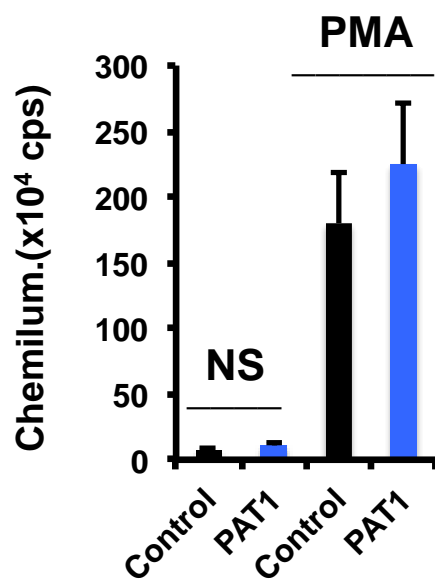
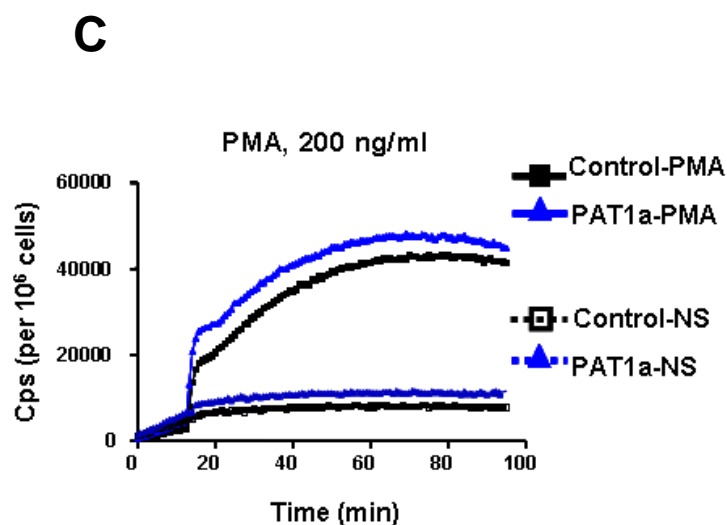
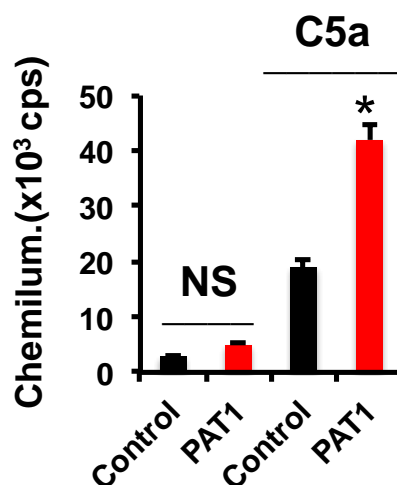
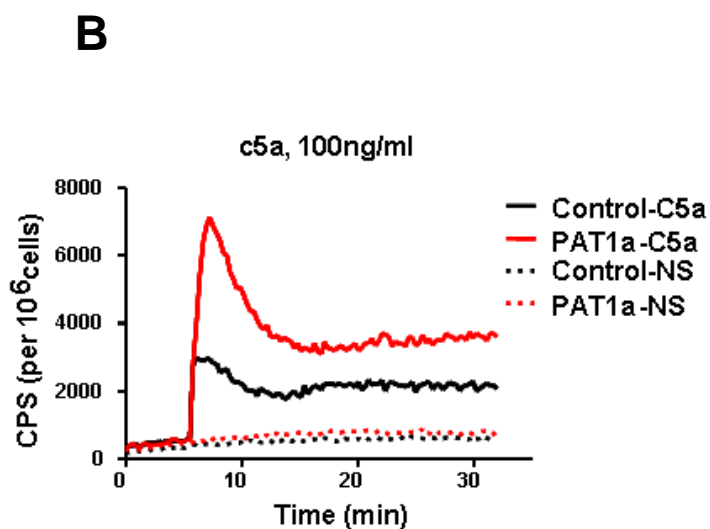
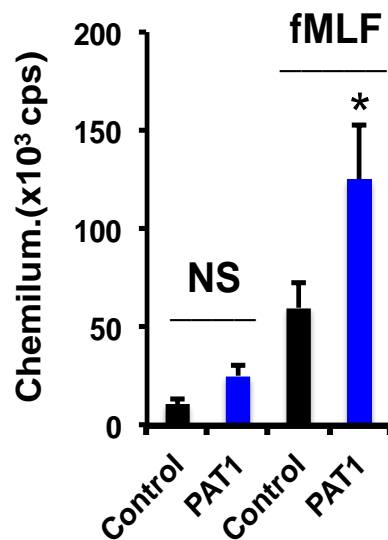
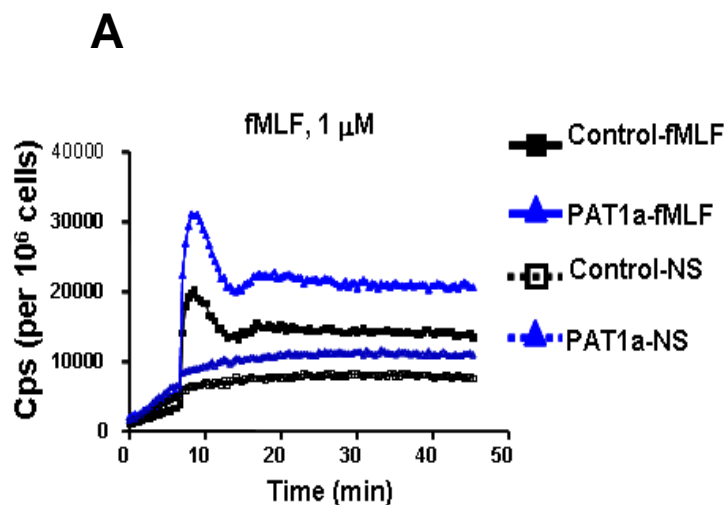
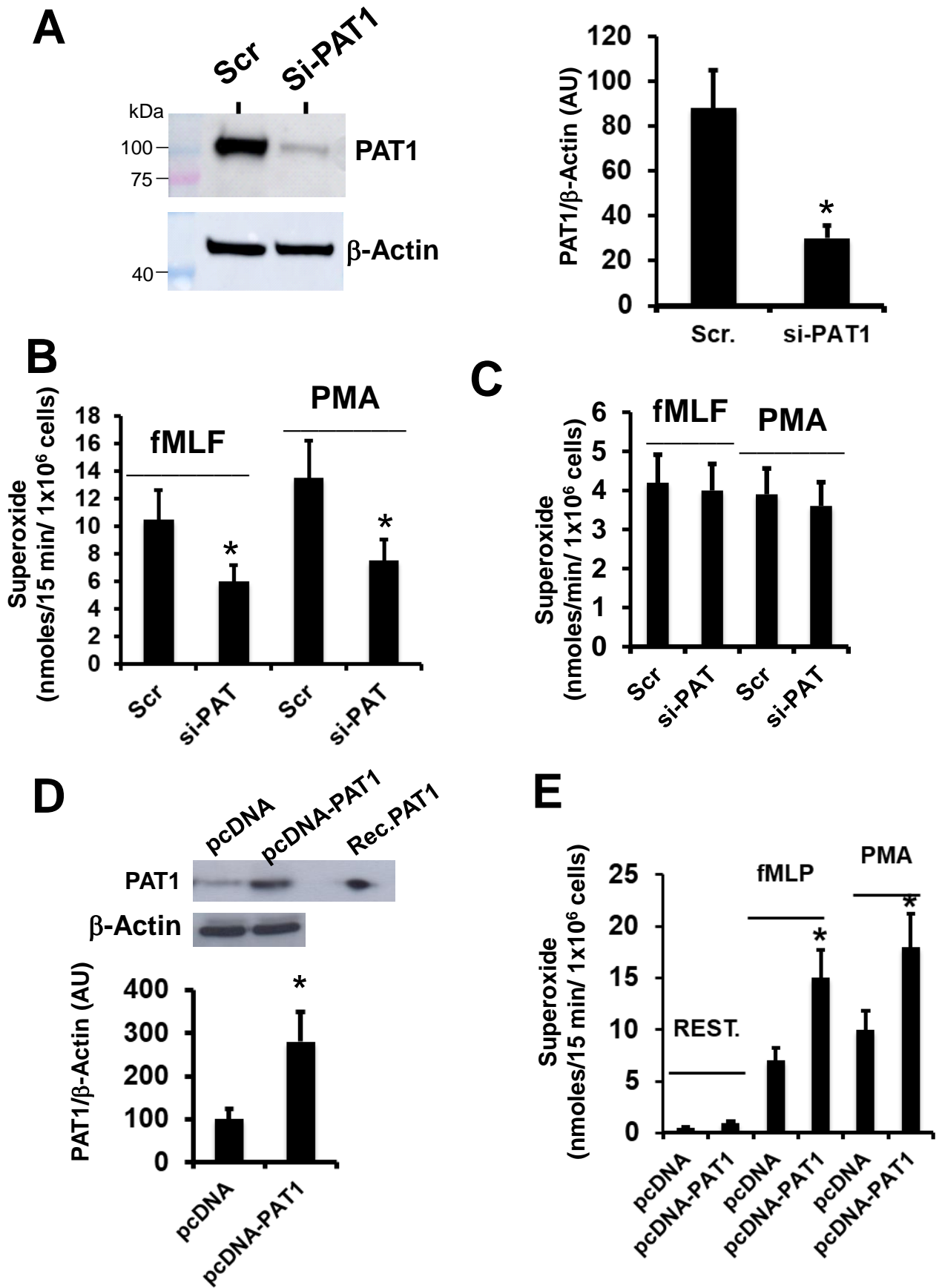


**Figure 6** (Arabi-Derkawi et al.)



## Supplemental Figure 1 (Arabi-Derkawi et al.)

```

                                     ccgtgcgccc
                                     gcgtggctgc
181 caccgcccct ccgaatcctc cggggccgca gaggggttcg ctacggaggg aggtgggggc
241 cttcgggagg aggaggcgga ggaggcggag gaggagggaa ggaagatggc ggccgtggaa
301 ctagagtgga tcccagagac tctctataac accgccatct ccgctgtcgt ggacaactac
361 atccgctccc gccgagacat ccgctccttg cccgagaaca tccagtttga tgtttactac
421 aagctttacc aacagggacg cttatgtcaa ctgggcagtg aattttgtga attggaagtt
481 tttgctaaag tactgagagc tttggataaa agacatttgc ttcattcattg ttttcaggct
541 ttgatggatc atggtgttaa agttgcttca gtcttggcct actcattcag taggcggtgc
601 tcttatatag cagaatcaga tgctgcagta aaggaaaaag ccattcagggt tggccttgtt
661 ttaggtggct ttctttcaga tgcaggctgg tacagtgatg ctgagaaagt ttttctgtcc
721 tgccttcagt tgtgtactct acacgatgag atgcttcatt ggtttcgtgc agtagaatgt
781 tgtgtgaggt tgcttcatgt gcgaaatgga aactgcaa atcatttggg tgaagaaaca
841 tttaaattag ctcagacata tatggataaa ctatcaaac atggccagca agcaaataaa
901 gctgcactct atggagaact gtgtgcactc ctatttgcaa aaagtcacta tgatgaggca
961 taaaa
```

**Fig. S1. Sequence of the clone which interacts with the p22phox-cytosolic region.** The sequence matched the homo sapiens kinesin light chain-related protein (PAT1) sequence (AF017782). The coding sequence started at nucleotide 286”atg...” shown in bold.

**Supplemental Figure 2 (Arabi-Derkawi et al.)**

**GST-Pull Down**

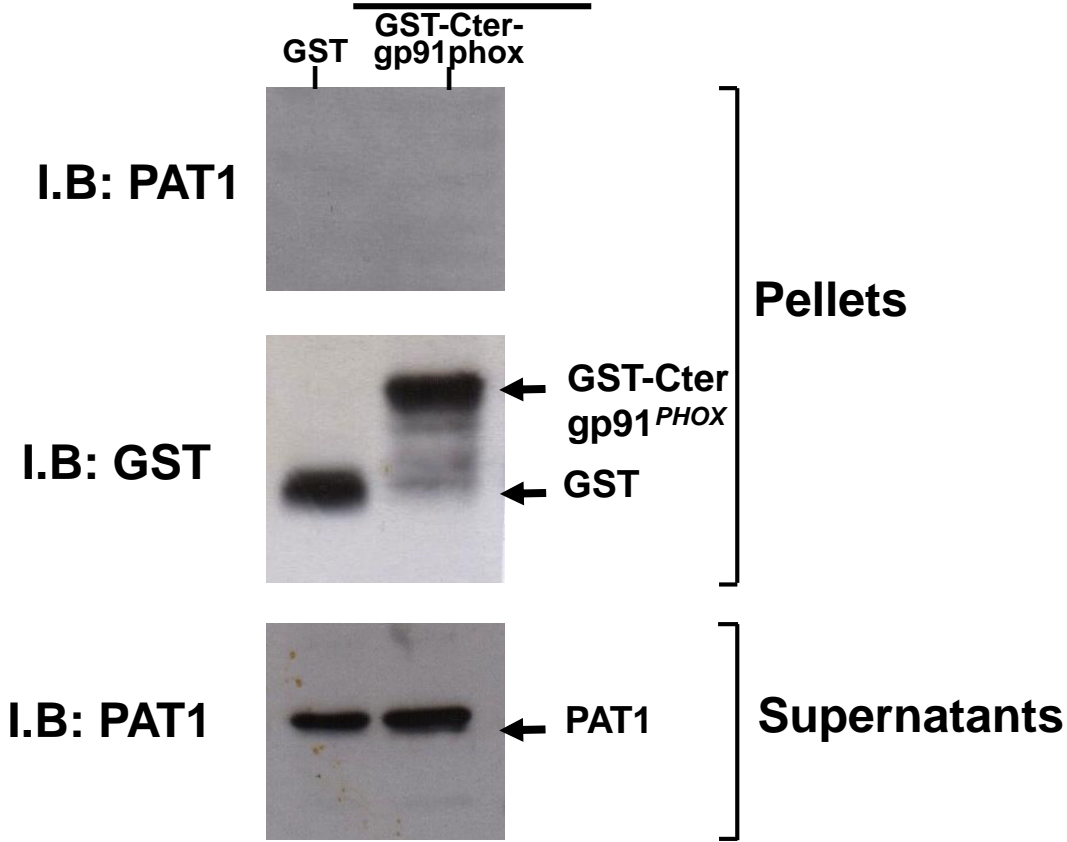


**Fig. S2. Gp91phox cytosolic tail does not interact with PAT1.** Recombinant human PAT1 (PAT1) was incubated with GST-gp91phox(aa291-570) or with GST protein and then with Glutathione (GSH)-agarose beads for 1h. After this incubation, the beads were washed three times and proteins were analyzed by SDS-PAGE and Western Blot using anti-GST or polyclonal anti-PAT1 antibodies. (repeated 3 times).

## Supplemental Figure 3 (Arabi-Derkawi et al.)

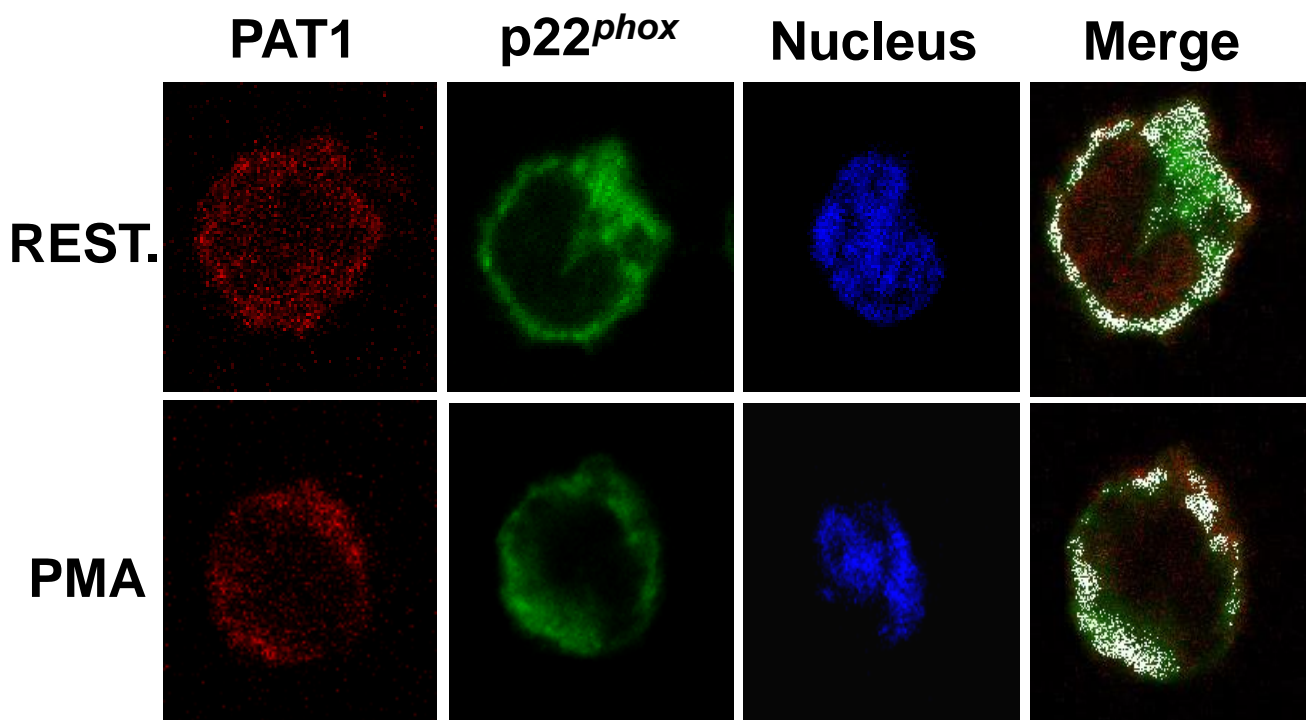


**Fig. S2 . PAT1 colocalization with p22phox in human monocytes.**

Monocytes in a resting state or treated with PMA (100 ng/ml), were prepared for confocal microscopy. Cells were incubated with a rabbit anti-p22phox antibody and a mouse anti-PAT1 antibody followed by incubation with Alexa Fluor 488-(green) conjugated goat anti-rabbit and Alexa Fluor 568 (red) conjugated goat anti-mouse. Nuclei were stained with TO-PRO-3. Stained cells were examined with a confocal microscope and the images were analyzed. The overlap of PAT1 and p22phox or of PAT1 and the nucleus is clearly seen as the white signal in the merged image.

# Supplemental Figure 4 (Arabi-Derkawi et al.)

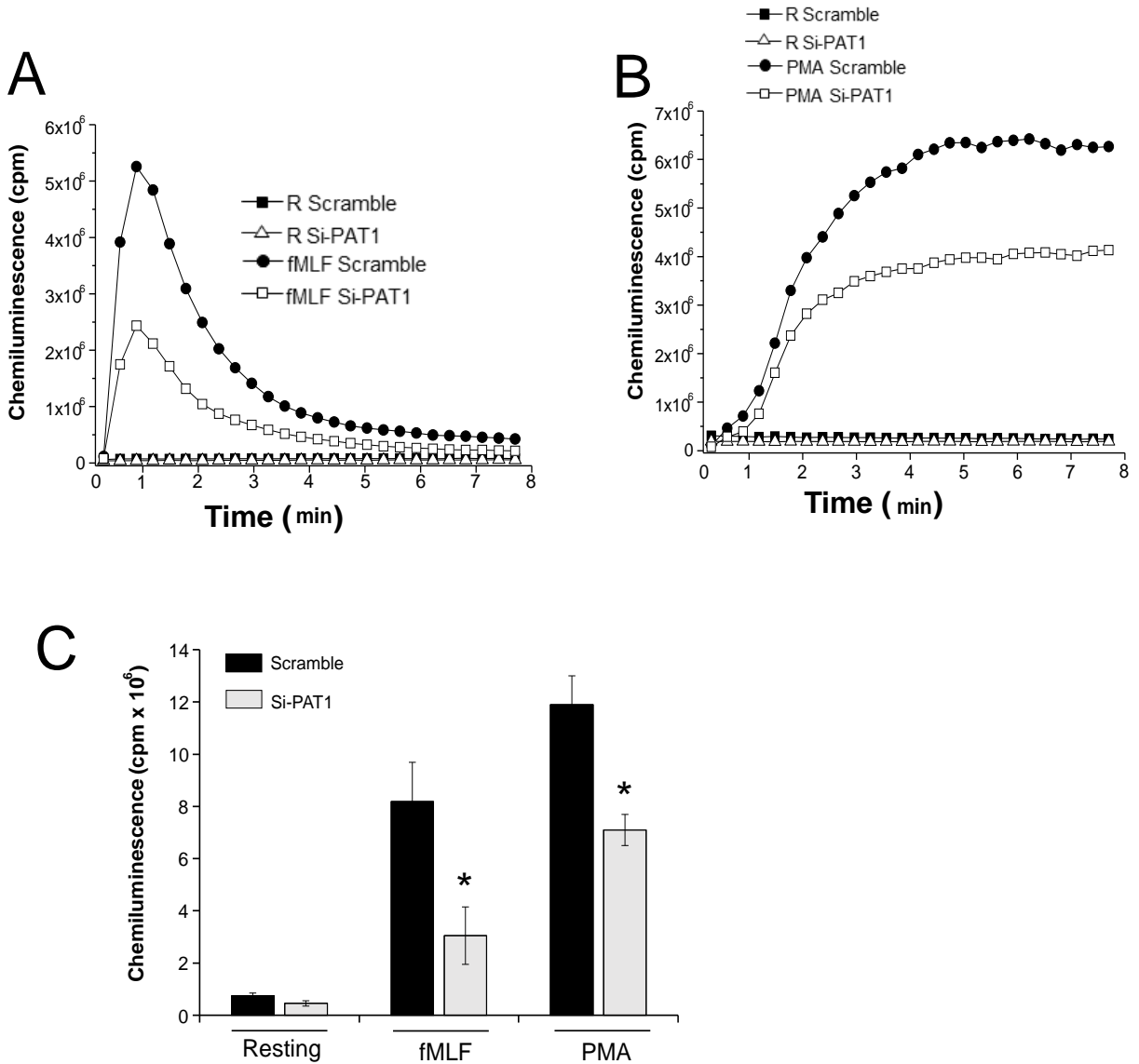


**Fig. S4. Effect of inhibition of PAT1 expression on human monocytes ROS production.** Human monocytes were freshly prepared and transfected with either scramble primers or siRNA PAT1 primers for 48h. ROS production was measured using luminol-amplified chemiluminescence in resting cells (R), fMLF ( $10^{-6}$  M)- (A) and PMA (100 ng/ml)(B)-stimulated cells treated with scramble and si-PAT1 RNA. Results from 3 experiments were quantified (mean  $\pm$  SEM, n= 3) \*  $p < 0.05$  as compared to scramble siRNA.